NEW INSIGHTS IN HUBER AND TV-LIKE REGULARIZERS IN MICROWAVE IMAGING

Funing Bai[1], Aleksandra Pižurica[1], Ann Franchois[2] and Wilfried Philips[1]

[1]Department of Telecommunications and Information Processing (IPI-TELIN-iMinds)
[2] Department of Information Technology (INTEC)
Ghent University, Belgium

ABSTRACT

In this paper we give new insights into quantitative microwave tomography with robust Huber regularizer and Gauss-Newton optimization. Firstly, we validate this approach for the first time on real electromagnetic measurements. Secondly, we extend the framework with a modified Huber function, which behaves like TV regularization. This is interesting for reconstructing piece-wise constant permittivities that appear in non-destructive testing of installations and other man-made objects.

Index Terms— inverse problem, microwave imaging, Huber function, sparsity, inverse scattering.

1. INTRODUCTION

Quantitative microwave imaging has the potential of reconstructing not only geometrical shapes but also exact permittivity profiles of unknown scattering objects. The images are obtained by illuminating the object with microwaves and by measuring the scattered field. Regularization is crucial for solving this ill-posed nonlinear inverse problem [1–5]. Multiplicative Smoothing (MS) [1] applies Tikhonov regularization in a multiplicative fashion. The Value Picking (VP) [2] regularizer favors piecewise constant targets with several distinct permittivities values. An edge preserving regularization in [3] was imposed on the real and imaginary part of the complex permittivity separately. Total variation (TV) was used as a multiplicative constraint in [4] and a Line Process model was employed in [5].

We introduced Huber regularization for this problem in our previous work [6] where we demonstrated encouraging first results on simulated data only. In this paper, we build further on this work, design an alternative TV-like regularization function within the same framework and we evaluate the whole approach on real electromagnetic measurements. The main novelties in this paper are: (1) extending the framework from [6] such that it can handle regularization that behaves like TV, which is of interest from theoretical point of view and practically because the new function proves to be even more effective for piecewise constant profiles that appear, e.g. in non-destructive testing of various installations

etc; (2) evaluating the complete framework of Huber regularization in microwave imaging for the first time on real data from electromagnetic measurements.

Scattering measurements of inhomogeneous targets from the Institute Fresnel, the so-called Fresnel database, are commonly used to test new algorithms in the inverse scattering community. A special issue of Inverse Problems [7] was devoted to reconstructions on these benchmark experimental data in order to enable fair comparison of the current and future methods using the same measurements. Moreover, validating inversion algorithms on experimental data is much more reliable than using simulations only, which are prone to inverse crime [8]. Reconstructions from the experimental data are quite challenging due to measurement noise and discretization noise as well as mismatch between the actual incident fields and their simulation in the forward solvers.

Our results on the experimental data motivate strongly the use of Huber regularization but also show potentials of extending the whole framework with other related functions. Especially, the modified Huber function (which behaves like TV regularization) demonstrates excellent performance on piece-wise constant profiles. This paper is organized as follows. In Section 2 the electromagnetic inverse scattering problem and Gauss-Newton method are revisited. An alternative regularization function, which is modified from the Huber function and which behaves similar to TV is discussed in Section 3 and experimental validations are presented in Section 4. Section 5 concludes the paper.

2. PROBLEM FORMULATION

As we described in [6], in order to reconstruct the permittivity profile $\boldsymbol{\varepsilon} = [\varepsilon_1, \cdots, \varepsilon_\nu, \cdots, \varepsilon_{N^\varepsilon}]$ of the object, an iterative method is used on a grid with N^ε square cells within a reconstruction domain $\mathcal{D}$, alternating between the forward and the update problem. In each step of the iterative method, simulated scattered fields $\mathbf{e}^{scat}(\boldsymbol{\varepsilon})$ are compared with the measured fields $\mathbf{e}^{meas}$ and the permittivity profile is updated based on this difference. This inverse problem is solved by minimizing a cost function

$$F(\boldsymbol{\varepsilon}) = F^{LS}(\boldsymbol{\varepsilon}) + \mu F^R(\boldsymbol{\varepsilon}) \qquad (1)$$

where $F^R(\boldsymbol{\varepsilon})$ is a regularization function, $\mu \geq 0$ is a regularization parameter and $F^{LS}(\boldsymbol{\varepsilon})$ is the least squares data fit:

$$F^{LS}(\boldsymbol{\varepsilon}) = \frac{\|\mathbf{e}^{meas} - \mathbf{e}^{scat}(\boldsymbol{\varepsilon})\|^2}{\|\mathbf{e}^{meas}\|^2} \tag{2}$$

$\mathbf{e}^{meas}$ and $\mathbf{e}^{scat}(\boldsymbol{\varepsilon})$ are N^d-dimensional vectors that represent the measured and the simulated scattered fields, respectively. We define the regularization function $F^R(\boldsymbol{\varepsilon})$ as

$$F^R(\boldsymbol{\varepsilon}) = \frac{1}{2} \sum_{\nu} \sum_{\nu' \in N_\nu} g_\gamma(\varepsilon_l - \varepsilon_{l'}) \tag{3}$$

where g_γ is a potential function with parameter γ and l' denotes a spatial position neighboring l in the neighborhood system N_l. We use 8 neighbors in 2D and 26 neighbors in 3D as a compromise between reconstruction quality and complexity.

As in [6], we consider minimization by an approximate line search along a Gauss-Newton descent direction, which requires a positive definite Hessian matrix. The complex permittivity in iteration k is updated as $\boldsymbol{\varepsilon}_{k+1} = \boldsymbol{\varepsilon}_k + \beta_k \Delta\boldsymbol{\varepsilon}_k$. β_k is calculated from the line search [2] and $\Delta\boldsymbol{\varepsilon}_k$ is obtained from

$$(\mathbf{J}_k^H \mathbf{J}_k + \lambda^2 \boldsymbol{\Sigma}_k^R)\Delta\boldsymbol{\varepsilon}_k = -(\mathbf{J}_k^H [\mathbf{e}^{scat}(\boldsymbol{\varepsilon}_k) - \mathbf{e}^{meas}] + \lambda^2 \boldsymbol{\Omega}_k^{R*}) \tag{4}$$

where $(.)^H$ stands for Hermitian transpose and $(.)^*$ denotes the complex conjugate. In the following, the subscript k is omitted. The factor $\mathbf{J}^H\mathbf{J} + \lambda^2\boldsymbol{\Sigma}^R$ is known as a Gauss-Newton Hessian matrix. The trade-off parameter λ is given by $\lambda^2 = \mu\|\mathbf{e}^{meas}\|^2$ [2]. $\mathbf{J}$ is the $N^d \times N^\varepsilon$ Jacobian matrix, which contains the derivatives of the scattered field components with respect to the optimization variables: $J_{d,l} = \partial e_d^{scat}/\partial\varepsilon_l$; $\boldsymbol{\Omega}^{R*}$ is an N^ε-dimensional vector that contains the derivatives of the regularizing function, $\Omega_l^{R*} = \partial F^R/\partial\varepsilon_l^*$; $\boldsymbol{\Sigma}^R$ is a $N^\varepsilon \times N^\varepsilon$ matrix $\Sigma_{l,l'}^R = \partial^2 F^R/\partial\varepsilon_{l'}\partial\varepsilon_l^*$.

We addressed this problem in [6], by deriving $\boldsymbol{\Omega}^{R*}$ and $\boldsymbol{\Sigma}^R$ for the Huber function. In this paper, we will not only validate this framework on real data, but we will also propose a new function in the same framework which behaves more effective on piecewise constant objects.

3. MODIFIED HUBER OR TV-LIKE REGULARIZATION

Microwave tomography is often applied in non-destructive testing of installations and other buried man-made objects with piece-wise constant permittivity profiles. For such problems total variation (TV) regularization is ideally suited. TV would correspond to defining g_γ in (3) as $g_{\gamma,TV}(\varepsilon_l - \varepsilon_{l'}) = |\varepsilon_l - \varepsilon_{l'}|$. Unfortunately, this function is non differentiable at $\varepsilon_l = \varepsilon_{l'}$ and hence it cannot be applied directly within our framework. Different solutions were proposed to work around this numerical problem, e.g., in [4, 9]. Here we propose another solution, which fits well with our framework
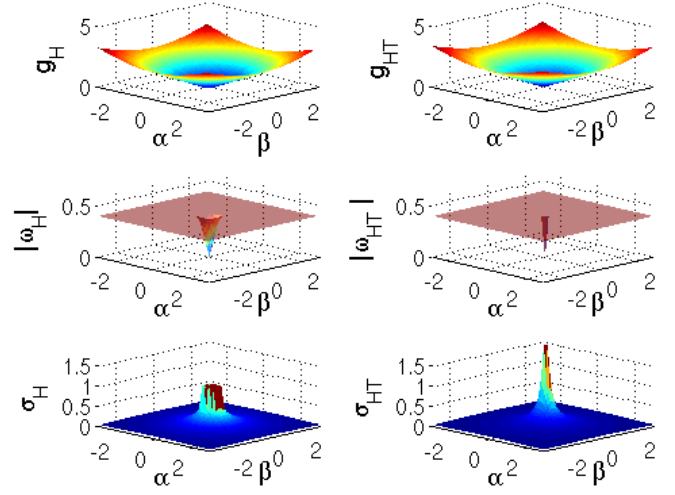
Fig. 1. The qualitative shape of the Huber and modified Huber functions in the complex domain, $\eta = \alpha + j\beta$.

from [6]. We start from $g_{\gamma,TV}$ and modify it only around $\varepsilon_l - \varepsilon_{l'} = 0$ to a quadratic form to ensure differentiability, resulting in

$$g_{\gamma,HT}(\varepsilon_l - \varepsilon_{l'}) = \begin{cases} |\varepsilon_l - \varepsilon_{l'}|^2 & , |\varepsilon_l - \varepsilon_{l'}| \leq \delta \\ \gamma|\varepsilon_l - \varepsilon_{l'}| & , otherwise \end{cases} \tag{5}$$

where $\delta \to 0$. With this function $F^R(\boldsymbol{\varepsilon})$ from (5) behaves like TV, just without suffering from the numerical problem at $\varepsilon_l = \varepsilon_{l'}$. It is interesting to note that this function can also be interpreted as a modified Huber function $g_{\gamma,H}(\eta) = |\eta|^2$ for $|\eta| \leq \gamma$ and $2\gamma|\eta| - \gamma^2$ otherwise.

To derive $\boldsymbol{\Omega}^{R*}$ and $\boldsymbol{\Sigma}^R$ in (4), g_γ in F^R will be substituted by (5). Note that ε in (5) is a complex number and hence $|\varepsilon_l - \varepsilon_{l'}|^2 = (\varepsilon_l - \varepsilon_{l'})(\varepsilon_l^* - \varepsilon_{l'}^*)$. It can be shown that

$$\Omega_l^{R*} = \frac{\partial F^R}{\partial\varepsilon_l^*} = \sum_{l' \in N_l} \omega_{l'}$$

$$\omega_{l'} = \begin{cases} (\varepsilon_l - \varepsilon_{l'}) & , |\varepsilon_l - \varepsilon_{l'}| \leq \delta \\ \dfrac{\gamma(\varepsilon_l - \varepsilon_{l'})}{2|\varepsilon_l - \varepsilon_{l'}|} & , otherwise \end{cases} \tag{6}$$

Consider next $\boldsymbol{\Sigma}^R$, which is a submatrix of the Hessian matrix, containing the second order derivatives of F^R. The diagonal elements of $\boldsymbol{\Sigma}^R$ are

$$\Sigma_{l,l}^R = \frac{\partial^2 F^R}{\partial\varepsilon_l\partial\varepsilon_l^*} = \sum_{l' \in N_l} \sigma_{l'} \tag{7}$$

$$\sigma_{l'} = \begin{cases} 1 & , |\varepsilon_l - \varepsilon_{l'}| \leq \delta \\ \dfrac{\gamma}{4|\varepsilon_l - \varepsilon_{l'}|} & , otherwise \end{cases}$$
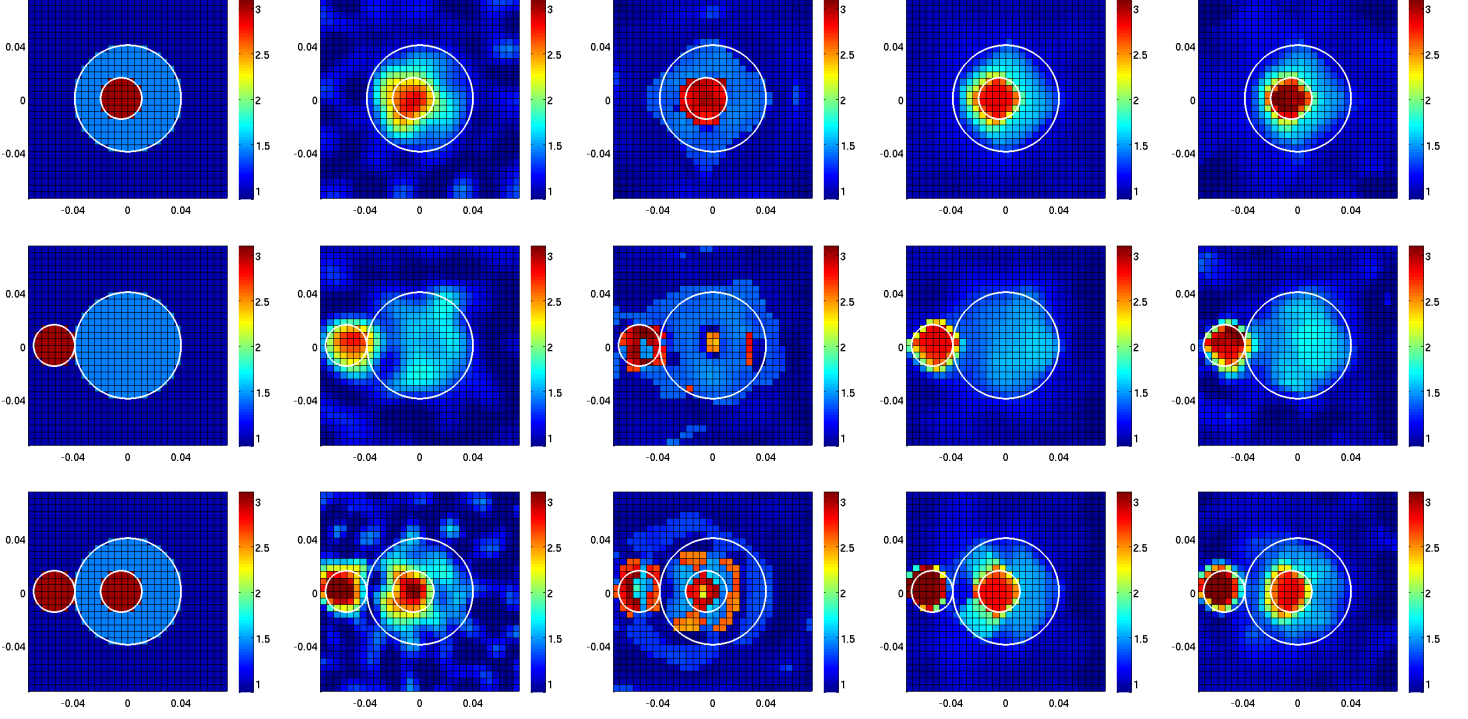
Fig. 2. Reconstruction results showing real part of the permittivity for different methods and three targets from the Fresnel database (top to bottom: FoamDielInt; FoamDielExt and TwinDiel). Left to right: reference (permittivity 1.45 ± 0.15 and 3 ± 0.3), MS, SRVP, Huber function and the modified Huber function.

and the non-diagonal elements are

$$\Sigma_{l,l'}^R = \frac{\partial^2 F^R}{\partial \varepsilon_{l'} \partial \varepsilon_l^*} \tag{8}$$

$$= \begin{cases} -1 & , |\varepsilon_l - \varepsilon_{l'}| \leq \delta \\ -\dfrac{\gamma}{4|\varepsilon_l - \varepsilon_{l'}|} & , otherwise \end{cases}$$

Now, equation (4) can be solved for TV-like regularization using (6)-(8), providing an alternative to Huber regularization from [6]. Note that the expressions (6)-(8) are nearly the same as those for the Huber function in [6], but one important difference is that an additional parameter δ exists now and this δ can be made arbitrarily small ($\delta \to 0$) without affecting the slope in the linear part of $g_{\gamma,HT}$ which is not the case with the Huber function $g_{\gamma,H}$. Fig. 1 illustrates the Huber function $g_H(\eta)$ and our TV-like function $g_{HT}(\eta)$ in the complex domain ($\eta = \alpha + j\beta$), together with the corresponding magnitude $|\omega(\eta)|$ and $\sigma(\eta)$ functions. Note that $|\omega|$ is an indication of the smoothing strength. $|\omega_H|$ increases with $|\eta|$ in the smoothing interval $|\eta| < \gamma$ and remains a constant, allowing limited (bounded) smoothing, outside this interval. $|\omega_{HT}|$ remains constant in the whole domain except around zero. The interaction σ, which determines the interaction between neighboring pixels also behaves differently for the two regularizations: σ_H is smaller for large $|\eta|$ and approaches 0

as $|\eta|$ goes to ∞, while σ_{HT} shows a very sharp interaction peak around zero. This way, TV-like function has a positive effect on the quality of the reconstruction for 'blocky' profiles like TV generally does. We optimize the regularization parameter γ and μ in (1) experimentally. For piece-wise constant objects $\gamma = 0.1$ is a good choice. For the regularization parameter μ, we obtained the same optimal value ($\sim 1\,10^{-3}$) in 2D and ($\sim 1\,10^{-4}$) in 3D for different targets and different antenna configurations in real data situation.

4. EXPERIMENTAL VALIDATION

We used three quasi lossless inhomogeneous targets from the Fresnel database: FoamDielInt, FoamDielExt and TwinDiel (shown in Fig. 2 and described with antenna configuration in [10]). We only use experimental data from measurements at 4GHz ($\lambda_0 = 7.49$cm). For each target, Multiplicative Smoothing (MS) [1], Step-wise relaxed value picking (SRVP) [2], Huber estimation [6] and the modified Huber function from this work are employed in independent reconstructions and the results are compared. The antenna positions are equally spaced on a circle with radius 1.67 m. The target is positioned in the center of this circle. For a transmitting antenna at $0°$, the receiving antenna can be positioned from $60°$ to $300°$. We only use 4 ($90°$ spaced)

Method	FoamDielint	FoamDielext	TwinDiel
MS [1]	15.35	14.73	18.04
SRVP [2]	11.13	17.00	22.09
Huber [6]	13.68	13.34	17.83
modified Huber	10.71	12.90	16.12

Table 1. Relative error $R = \parallel \varepsilon^{rec} - \varepsilon^{ref} \parallel^2 / \parallel \varepsilon^{ref} \parallel^2$ (%) for the reconstructed permittivities from Fig. 2 with the different methods. ε^{rec} and ε^{ref} are reconstructed and reference permittivity profiles, respectively.

transmitting antennas (9 (40° spaced) for TwinDiel), each with TM and TE polarizations, and 9 (30° spaced) receiving antennas, resulting in a data vector $\mathbf{e}^{meas}$ of length $N^d = 108$ (243 for TwinDiel) complex numbers. A calibration is applied to match amplitude and phase between measured and simulated fields. For each incidence, the measured scattered field values are multiplied with a complex factor, which is the ratio of the simulated and the measured incident fields at the receiver located opposite to the source. This number of data points is sparse by the criterion of [11], which is of interest in terms of computation time.

The reconstruction domain in the inverse solver is discretized in 30×30 square inverse problem cells (edge size = 5 mm $\approx \lambda_0/15$), yielding a total of 900 permittivity unknowns. To solve the forward problems, each inverse problem cell is subdivided in $2 \times 2 = 4$ forward problem cells, which have the same permittivity. In our experiments, BICGSTAB-FFT (bi-conjugate gradient stabilized method-Fast Fourier Transform) forward solver is used to accelerate the calculations.

With the chosen antenna configuration (4 transmitting and 9 receiving antennas, i.e., 108 data points), the reconstruction with each of the analyzed methods takes around 20 min on a six-core Intel i7 980x processor (3.33GHz) with 24GByte memory (threads = 8). With 8 transmitting and 241 receiving antennas (5784 data points), the reconstruction time is 20 hours. In both cases, the same stopping criterion is used ($F^{LS} = 10^{-3}$ or maximum 20 iterations).

Fig. 2 shows the reconstructions with the different methods using 4 (9 for TwinDiel) transmitting and 9 receiving antennas. Only the real parts of the permittivities are shown, since the imaginary parts are almost zero. The parameters for MS and SRVP were set as in [12]: $\mu = 2 \times 10^{-3}$ for MS and $\mu = 3$ for SRVP. Like with simulated data in [6], MS oversmooths the targets, especially at edges. SRVP cannot reconstruct well the objects from such a small number of data points (see the two bottom images in the middle column). The results of our Huber regularization and modified Huber function are much closer to the ground truth. Table 1 shows the corresponding reconstruction errors. This provides for the first time validation of our original framework from [6] with robust statistical regularization on actual electromagnetic measurements and motivates clearly the use of this approach. Moreover, the extension with modified Huber

(a) Huber   (b) modified Huber

(a1) Huber   (b1) modified Huber
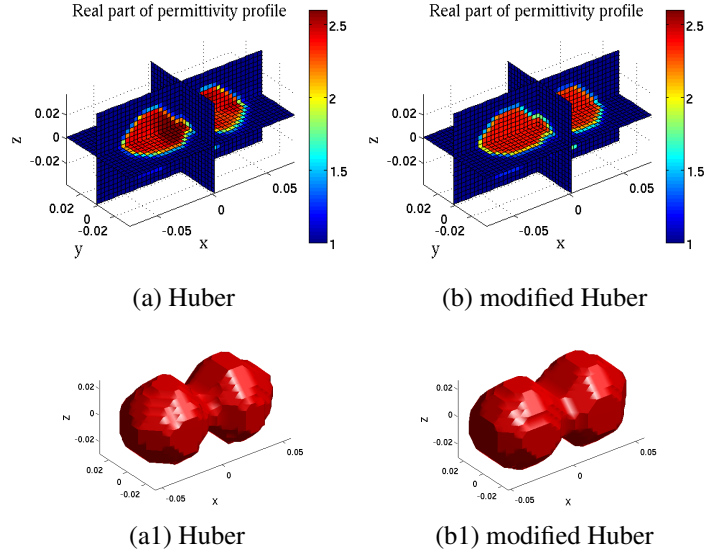
Fig. 3. Reconstructions of Two Spheres at 4GHz and a 3D view of the surface.

function proposed in this paper proves to be even more effective in the reconstruction of piecewise constant objects.

To test the effectiveness of our inversion algorithms in even more challenging scenario with 3D real data, we select one 3D target–Two Spheres from the Fresnel database described with antenna configuration in [13]. The only difference is that we use 4 receiving dipoles compared to 36 in original data, resulting in a data vector $\mathbf{e}^{meas}$ of length $N^d = 479$ sparse numbers of data points. The reconstruction domain in the inverse solver is discretized in $40 \times 20 \times 20$ cube inverse problem cells (16000 permittivity unknowns). Using 479 data points and the same hardware parameters as in the 2D case, the reconstruction takes 40 minutes in 10 iterations or with a stop criterion $F^{LS} = 10^{-3}$. The reconstruction from Huber regularization and modified Huber function are shown in Fig. 3. The shape is well reconstructed and the value is very close to the reference value which is $2.6 - j0$.

5. SUMMARY

We extended and gave new insights into the framework of quantitative microwave imaging with robust Huber regularization. We showed how this framework can be used with other related functions, by modifying the Huber function such that the resulting regularization behaves like TV regularization, and without numerical problems. We also demonstrated for the first time the results of this complete framework in real electromagnetic measurements, showing its potentials in sparse measurements with relatively few receiving antennas.

6. REFERENCES

[1] J. De Zaeytijd and A. Franchois, "Three-dimensional quantitative microwave imaging from measured data with multiplicative smoothing and value picking regularization," *Inverse Probl.*, vol. 25, no. 2, pp. 024004, 2009.

[2] J. De Zaeytijd, A. Franchois, and J.M. Geffrin, "A new value picking regularization strategy - application to the 3-D electromagnetic inverse scattering problem," *IEEE Trans. Antennas Propag.*, vol. 57, no. 4, pp. 1133 –1149, April 2009.

[3] P. Lobel, C. Pichot, L. Blanc-Feraud, and M. Barlaud, "Microwave imaging: Reconstructions from experimental data using conjugate gradient and enhancement by edge-preserving regularization," *Int. Journal of Imaging Syst. and Technol.*, vol. 8, no. 4, pp. 337–342, 1997.

[4] A. Abubakar and P.M. Van Den Berg, "Total variation as a multiplicative constraint for solving inverse problems," *IEEE Trans. Image Process.*, vol. 10, no. 9, pp. 1384 –1392, Sep 2001.

[5] S. Caorsi, G.L. Gragnani, S. Medicina, M. Pastorino, and G. Zunino, "Microwave imaging based on a Markov random field model," *IEEE Trans. Antennas Propag.*, vol. 42, pp. 293–303, Mar 1994.

[6] F. Bai, A. Pižurica, S. Van Loocke, A. Franchois, D. De Zutter, and W. Philips, "Quantitative microwave tomography from sparse measurements using a robust Huber regularizer," in *In IEEE Int. Conf. Image Processing (ICIP)*, October 2012, pp. 2073–2076.

[7] Kamal Belkebir and Marc Saillard, Eds., *Special section on testing inversion algorithms against experimental data: inhomogeneous targets*, vol. 21, Special issue of Inverse Problems, 2005.

[8] D Colton and R Kress, *Inverse Acoustic and Electromagnetic Scattering Theory*, Springer, 1992.

[9] Andrea Borsic, Brad M. Graham, Andy Adler, and William R. B. Lionheart, "In vivo impedance imaging with total variation regularization," *IEEE Trans. Med. Imaging*, pp. 44–54, 2010.

[10] J. Geffrin, P. Sabouroux, and C. Eyraud, "Free space experimental scattering database continuation: experimental set-up and measurement precision," *Inverse Problems*, vol. 21, no. 6, pp. S117, 2005.

[11] O.M. Bucci and T. Isernia, "Electromagnetic inverse scattering: Retrievable information and measuement strategies," *Radio Science*, vol. 32, pp. 2123–2137, 1997.

[12] S. Van den Bulcke, *A 2.5D electromagnetic quantitative inverse scattering technique to visualize concealed objects using millimeter waves*, Phd thesis, Ghent University. Faculty of Engineering, 2010.

[13] J M Geffrin and P Sabouroux, "Continuing with the Fresnel database: experimental setup and improvements in 3D scattering measurements," *Inverse Problems*, vol. 25, no. 2, pp. 024001, 2009.